High-Efficiency Broadband High-Harmonic Generation from a Single Quasi-Phase-Matching Nonlinear Crystal

Bao-Qin Chen, Chao Zhang, Chen-Yang Hu, Rong-Juan Liu, and Zhi-Yuan Li*
Laboratory of Optical Physics, Institute of Physics, Chinese Academy of Sciences, P.O. Box 603, Beijing 100190, China
(Received 6 February 2015; published 20 August 2015)

Nonlinear frequency conversion offers an effective way to expand the laser wavelength range based on birefringence phase matching (BPM) or quasi-phase-matching (QPM) techniques in nonlinear crystals. So far, efficient high-harmonic generation is enabled only via multiple cascaded crystals because of the extreme difficulty to simultaneously satisfy BPM or QPM for multiple nonlinear up-conversion processes within a single crystal. Here we report the design and fabrication of a chirped periodic poled lithium niobate (CPPLN) nonlinear crystal that offers controllable multiple QPM bands to support 2nd–8th harmonic generation (HG) simultaneously. Upon illumination of a mid-IR femtosecond pulse laser, we observe the generation of an ultrabroadband visible white light beam corresponding to 5th–8th HG with a record high conversion efficiency of 18%, which is high compared to conventional supercontinuum generation, especially in the HG parts. Our CPPLN scheme opens up a new avenue to explore and engineer novel nonlinear optical interactions in solid state materials for application in ultrafast lasers and broadband laser sources.

DOI: 10.1103/PhysRevLett.115.083902 PACS numbers: 42.65.Ky, 77.80.Dj

Since the invention of the laser, nonlinear optics has become a popular and efficient routine for expanding the frequency window of lasers from ultraviolet to visible, infrared, and terahertz bands, and for generating broadband coherent light sources and ultrafast pulse lasers [1–7]. These are achieved by the interaction of laser light (continuous or pulse) with nonlinear crystals. Different up-conversion processes such as second-harmonic generation (SHG), sum-frequency generation (SFG), and third-harmonic generation (THG) allow expansion to short wavelength bands [8–17]. To maintain high-efficiency frequency conversion, phase matching must be satisfied for light waves of different frequencies propagating and interacting within the nonlinear crystal, either via the birefringence phase matching (BPM) or quasi-phase-matching (QPM) scheme [1–7].

SHG can be readily realized in a single crystal [1–9], and THG can also be realized in a single crystal either via the cascaded process of SHG and SFG [10–13] or directly via the third-order nonlinear interaction [14]. However, it would become more and more difficult, or even impossible, to realize high-harmonic generation (HHG) in a single crystal, because more and more nonlinear up-conversion processes must be simultaneously adopted with phase matching. Instead, a chain of two or more individual nonlinear crystals with cascaded SHG and SFG is used [15–17], but with a complicated experimental setup and low conversion efficiency. Another way to realize HHG is via the interaction of a high peak-power ultrafast pulse laser with a dilute atomic vapor and plasma [18–20]. Very high order HHG with a wavelength in the extreme ultraviolet [21–24] and x-ray bands [25] has been achieved, but with even lower conversion efficiency. In this work we report simultaneous 5th–8th harmonic generation (HG) from a single chirped periodic poled lithium niobate (CPPLN) nonlinear crystal, which enables the QPM up-conversion of a mid-IR pulse laser into visible ultrabroadband white light with a record-high conversion efficiency of 18%.

A periodic or quasiperiodic nonlinear crystal exhibits a series of discrete reciprocal lattice vectors (RLVs) in the Fourier-transform spectrum [4–8] with a large effective nonlinear susceptibility χ_{eff} [9,26,27]. Each RLV line can only be adopted for the QPM SHG or SFG at a specific frequency ω of the fundamental-wave (FW) pump light. To achieve THG in such a single crystal via cascaded SHG ($\omega + \omega \rightarrow 2\omega$) and SFG ($\omega + 2\omega \rightarrow 3\omega$) [10,11], two RLV lines of sufficiently large χ_{eff}, one for SHG, the other for SFG, must be supported, and already this is not an easy thing. It would then be almost impossible to achieve HHG using these crystals, because now more and more RLV lines that match all the cascaded processes and at the same time have sufficiently large χ_{eff} must be available. Because of these difficulties, the experimental realization of efficient HHG via multiple cascaded QPM processes from a single nonlinear crystal has not yet been successful.

Things can become much easier when the RLV lines are expanded into RLV bands of finite bandwidth and large χ_{eff} to allow broadband QPM, because now one can easily find two RLV lines that enable cascaded SHG and SFG for specific pump FW light from these QPM bands. Recently, we introduced chirped modulation into a periodic poled lithium niobate crystal to create a CPPLN crystal, where each discrete QPM line is expanded into a QPM band of finite bandwidth [13]. The center and bandwidth of these

QPM bands can be easily designed to support cascaded SHG and SFG and allow simultaneous broadband SHG and THG [13]. Moreover, the broadband QPM in CPPLN enables SHG and SFG up-conversion of the whole broadband FW light of a femtosecond pulse laser. Because the femtosecond laser pulse has a very high peak power, the conversion efficiency can be greatly enhanced compared with the usual narrow-band pump. In the following we will show that such a CPPLN crystal works perfectly well for high-efficiency HHG under the pump of a mid-IR femtosecond pulse laser.

The CPPLN nonlinear crystal has a modulation period of the nonlinear susceptibility varying along the propagation direction described by $\Lambda(z) = \Lambda_0/[1 + (D_g\Lambda_0 z/2\pi)]$, where $\Lambda_0 = 2\pi/\Delta k_0$ and D_g is the chirp rate. Following Ref. [13], we chose a structure with an optimized chirp rate of $D_g = 1.2$ to ensure a balanced broadband and high conversion efficiency HHG process. The wave vector mismatch $\Delta k_0 = 4\pi[n_2(\lambda_0) - n_1(\lambda_0)]/\lambda_0$ is defined for SHG at a selected value of the fundamental wavelength, which is $\lambda_0 = 3.8$ μm, located well within the spectral band of the mid-IR femtosecond pump light. As shown in Fig. 1(a), the CPPLN crystal has a fixed width of negative domain, $l_- = 15.7$ μm and a varying length of positive domain, l_+, and the poled period is $\Lambda(z) = l_+(z) + l_-$. Photographs of the CPPLN sample, fabricated using an electric poling technique [13], are displayed in Figs. 1(b) and 1(c). The sample has a total length of about $L = 16$ mm and the lattice pitch size gradually decreases from 34.04 μm at the left end to 28.18 μm at the right end.

The calculated Fourier-transform spectrum of the sample is displayed in Fig. 2(a). The spectrum exhibits five relevant RLV bands with considerable strength in χ_{eff}, which are located at [0.1,0.3] for band B1, [0.3.0.5] for band B2, [0.5,0.8] for band B3, [0.8,1.2] for band B4, and [1.2,2.0] for band B5, all in units of μm^{-1}. Band B1 has the highest strength in χ_{eff} and still has a sufficiently broad RLV bandwidth, while the other four bands have relatively smaller strength in χ_{eff} but have very broad RLV bandwidth. This unique spectral feature will allow for efficient HHG from such a CPPLN sample via a series of cascaded QPM three-wave mixing (SHG and SFG) processes. Besides, the spectral curves exhibit some noisy lines due to the finite length of the sample.

To clearly illustrate the mechanism of QPM for SHG and SFG in CPPLN, we calculate and plot the phase-mismatching curve of the $LiNbO_3$ material (versus the FW wavelength) for SHG and SFG alongside the Fourier spectral curves (versus the RLV) in Figs. 2(b)–2(f). The wave-vector mismatch Δk_i for different nonlinear frequency conversion processes that are responsible for 2nd–8th HG in these figures is defined in Table I. It can be seen clearly from Fig. 2(b) that in the entire band of the pulse laser FW pump light, 3400–3800 nm, the desired wave-vector mismatching quantity for the Δk_1 (SHG) and Δk_2 (SFG) processes is completely covered by band B1. This means that SHG and THG are enabled by QPM over the entire band of the pulse laser pump light. In other words, all the energies of the mid-IR femtosecond pulse

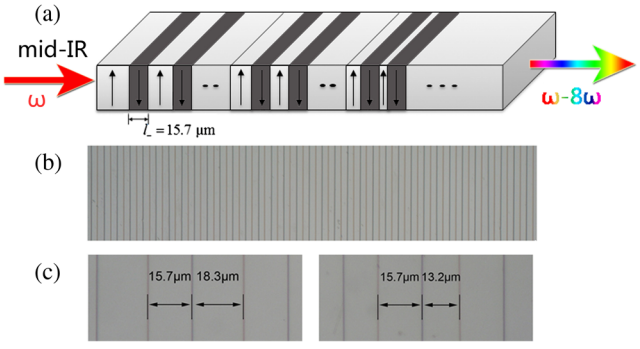

FIG. 1 (color online). Design of CPPLN for HHG under pump of a mid-IR femtosecond pulse laser. (a) Schematic diagram of the structural geometry of a CPPLN structure used to enable HHG via multiple-band QPM processes. The up or down arrows indicate positive or negative domains, respectively. (b) Microscopic image of the etched sample surface of a typical 1D CPPLN structure. (c) Expanded views of two small segments from the left-hand and right-hand portions of the CPPLN sample.

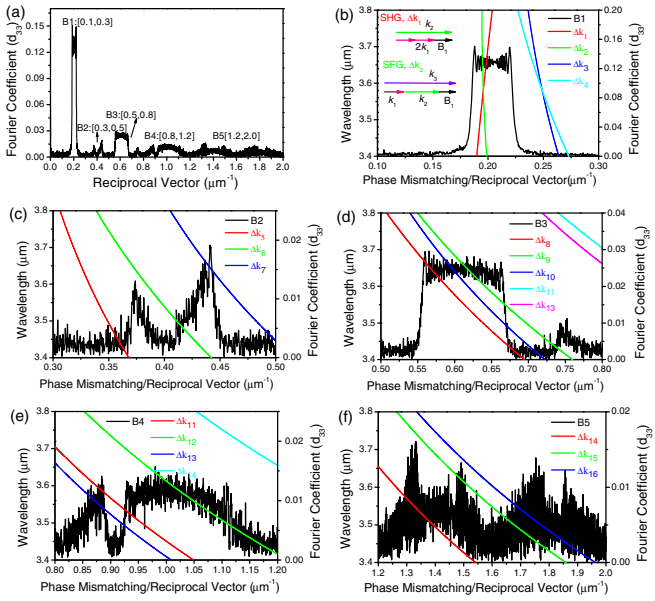

FIG. 2 (color online). QPM schemes in CPPLN for HHG based on broadband three-wave mixing as SHG and SFG. (a) Calculated distributions of the effective nonlinear coefficient as functions of the RLVs for the CPPLN sample, which are separated into five QPM bands. (b)–(f) Combined plots of the phase-mismatch curves for various three-wave mixing processes in a homogeneous $LiNbO_3$ crystal and the effective nonlinear coefficient curve for the CPPLN structure in 2nd–8th HG processes. Overlap between the two curves within a given wavelength band of the mid-IR FW means that QPM is satisfied to support efficient three-wave mixing. The inset figures in panel (b) explicitly indicate the QPM process leading to SHG and THG through SFG.

TABLE I. Definition of the wave-vector mismatch Δk as used in Fig. 2 for the different nonlinear three-wave mixing processes that contribute to various-order HHG. k_i is the wave number of the ith HG wave within a $LiNbO_3$ crystal given by $k_i = i \times k_0 \times n(\lambda_i)$, where k_0 is the wave number of the FW in vacuum and $n(\lambda_i)$ is the refractive index of $LiNbO_3$ at the ith HG wavelength λ_i.

HHG	Phase mismatching in three-wave mixing processes	QPM band
2nd HG	$\Delta k_1 = k_2 - 2k_1$	B1
3rd HG	$\Delta k_2 = k_3 - k_2 - k_1$	B1
4th HG	$\Delta k_3 = k_4 - k_3 - k_1, \Delta k_4 = k_4 - 2k_2$	B1
5th HG	$\Delta k_5 = k_5 - k_4 - k_1, \Delta k_6 = k_5 - k_3 - k_2$	B2
6th HG	$\Delta k_7 = k_6 - k_5 - k_1, \Delta k_8 = k_6 - k_4 - k_2, \Delta k_9 = k_6 - 2k_3$	B2, B3
7th HG	$\Delta k_{10} = k_7 - k_6 - k_1, \Delta k_{11} = k_7 - k_5 - k_2, \Delta k_{12} = k_7 - k_4 - k_3$	B3, B4
8th HG	$\Delta k_{13} = k_8 - k_7 - k_1, \Delta k_{14} = k_8 - k_6 - k_2, \Delta k_{15} = k_8 - k_5 - k_3, \Delta k_{16} = k_8 - 2k_4$	B4, B5

laser in different wavelengths can efficiently participate in SHG and THG within the CPPLN sample. Obviously this feature, together with the large χ_{eff} in band B1 (around $0.14d_{33}$, with $d_{33} = 27$ pm/V), is very beneficial for reaching a high conversion efficiency of SHG and THG and in turn for igniting efficient HHG, as SHG and THG can now become the starting point to create other higher-order nonlinear up-conversion processes, which indeed can happen according to the analyses made in Figs. 2(b)–2(f).

It can be seen from Fig. 2(b) that for the Δk_3 and Δk_4 processes that contribute to 4th HG, only the phase mismatching curve of Δk_3 has a narrow-band overlapping with band B1 at its large RLV edge ~0.3 μm^{-1}. As a result, only the long-wavelength part (around 3800 nm) of the energy of the femtosecond pulse laser can be used to ignite the 4th HG. Because of this narrow-band feature, the overall efficiency of the 4th HG will not be high. According to Figs. 2(c)–2(f), band B2 is responsible for 5th HG dominantly through QPM for the Δk_6 process within the RLV band 0.37–0.45 μm^{-1} and the associated FW pump wavelength range 3650–3400 nm, while the Δk_5 process contributes negligibly. Considering the compromise among the modest-width QPM band, relatively small χ_{eff} ($\sim 0.01d_{33}$), and high intensity second harmonic wave and third harmonic wave enabled by band B1, 5th HG can still take place from the CPPLN sample with considerable conversion efficiency.

Sixth HG can be enabled by QPM via the Δk_7 process within the RLV band 0.415–0.45 μm^{-1} in band B2 and FW band 3800–3600 nm via the Δk_8 process within 0.55–0.67 μm^{-1} in band B3 and FW band 3700–3400 nm, and via the Δk_9 process within 0.55–0.67 μm^{-1} in band B3 and FW band 3800–3550 nm. Because the sample supports broadband QPM and a relatively large χ_{eff} ($0.02d_{33} - 0.03d_{33}$) for all the three processes, it is expected that the efficiency for 6th HG can be at a high level. Three QPM enabled processes contribute to 7th HG, which are the Δk_{10} process within 0.55–0.67 μm^{-1} in band B3 ($\chi_{\text{eff}} \sim 0.03d_{33}$) and FW band 3800–3500 nm, the Δk_{11} process within 0.74–1.05 μm^{-1} covering bands B3 and B4 ($\chi_{\text{eff}} \sim 0.01d_{33} - 0.015d_{33}$) and FW band 3800–3400 nm, and via the Δk_{12} process within 0.85–1.2 μm^{-1} in band B4 ($\chi_{\text{eff}} \sim 0.01d_{33}$) and FW band 3800–3400 nm. All three processes cover a broad QPM band and pump light wavelength band, so the efficiency may also be high. As to 8th HG, four QPM enabled processes Δk_{13}, Δk_{14}, Δk_{15}, and Δk_{16} via bands B4 and B5 can make contributions. Because of the compromise among the high-order nonlinear interaction, the relatively low $\chi_{\text{eff}}(\sim 0.01d_{33})$, and the available broad QPM band and pump wavelength band, the efficiency of 8th HG might not be high, but it is still observable.

We measured and analyzed HHG from the CPPLN sample using the apparatus shown in Fig. 3(a). A femtosecond optical parametric amplification laser served as the pump source, which can produce 1300 nm center-wavelength near-IR band, 2100 nm center-wavelength IR band, and 3600 nm center-wavelength mid-IR band laser pulses. To ensure that only the mid-IR band (3400–3800 nm)

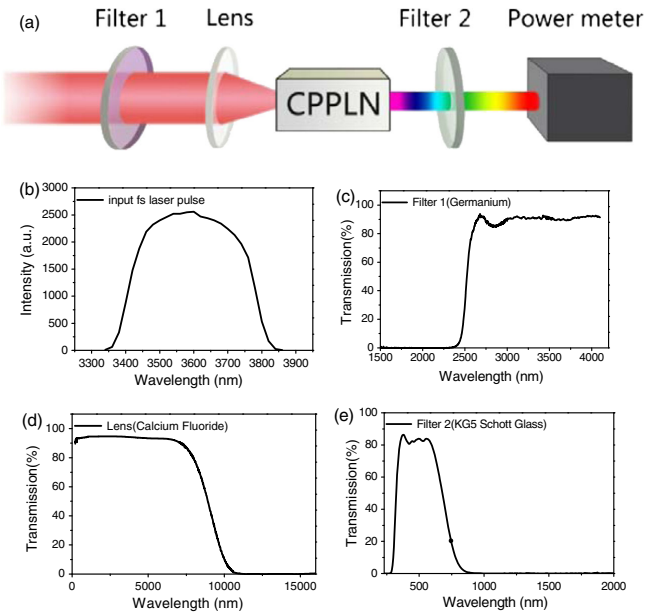

FIG. 3 (color online). Experimental setup of HHG from the CPPLN sample. (a) Schematic of the experimental setup. (b) Measured spectrum of the input femtosecond pulse laser pump source. (c) The transmission spectrum of filter 1, showing a short-wavelength cutoff of 2400 nm. (d) The transmission spectrum of the lens. (d) The transmission curve of filter 2.

femtosecond laser participated in pumping HHG and to clarify the conversion efficiency measurement of the 5th–8th HG, which would occur in the visible band, appropriate filters and a lens were carefully selected for the nonlinear optical measurement setup. As illustrated in Figs. 3(c)–3(e), their performance is quite satisfactory. The final pump light entering the CPPLN sample was then a mid-IR femtosecond pulse laser with a pulse full width at half maximum of 115 fs, average power of 20 mW, bandwidth of 3400–3800 nm, repetition rate of 1 kHz, and peak power of 0.17 GW [Fig. 3(b)]. This power level did not cause any damage to the CPPLN sample.

The mid-IR femtosecond pump laser was weakly focused with a spot radius of about 200 μm and coupled into the polished end of the sample with a peak intensity of 120 GW/cm^2 and a nearly plane-wave field profile. A very bright white light beam was observed with the naked eye. To analyze the spectrum of the white light beam, we first used a gold grating (1800 lines/mm) for a qualitative assessment. As illustrated in Fig. 4(a), the zeroth-order diffraction beam and −1st-order diffraction beam were observed. The zeroth-order diffraction beam, which is a direct reflection of the incident beam, manifests a very regular white light spot that maintains the original profile of the pump light beam [Fig. 4(b)]. The −1st-order diffraction beam, as illustrated in Fig. 4(c), looks like a color ribbon composed of a continuous color band ranging from purple to red.

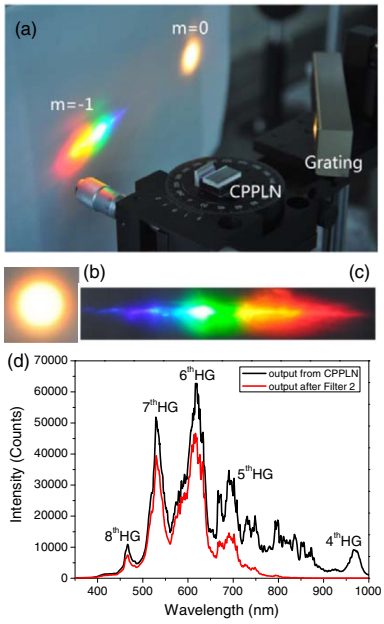

FIG. 4 (color online). Measurement results of HHG from the CPPLN sample. (a) Photo picture of a simple grating setup used to observe the spectral component of the output HHG light beam with the naked eye. The observation screen records (b) the zeroth-order reflection beam and (c) the −1st-order diffraction beam. (d) The spectrum of the output HHG signals measured before and after filter 2 in the visible and near-IR bands.

Clearly, this feature reflects the fact that the output light from the CPPLN crystal is an ultrabroadband visible light beam diffracted by the strongly dispersive grating. We further used an optical spectrometer to make an accurate spectral analysis over this output white light beam and found that the output light signal covers a series of visible and near-IR bands corresponding to 2nd–8th HG of the mid-IR FW light. The measured spectrum curve is plotted in Fig. 4(d) (black line) for wavelengths ranging from 350 to 1000 nm and exhibits five discrete bands with peaks located at around 966, 691, 616, 530, and 466 nm, respectively, which obviously correspond to 4th–8th HG of the FW light.

To quantify the conversion efficiency, we used a power meter placed after the bandpass colored glass filter (filter 2) to measure the power of the visible light signal and recorded a value of 1.69 mW. At the same time, we carefully analyzed the spectrum of the output light after filter 2, which is also plotted in Fig. 4(d) (red line) for the sake of comparison. The new spectral curve matches well with the spectrum of the directly output HHG signal (black line) when considering the transmittance performance of filter 2 [Fig. 3(e)]. The new spectrum was used as a reference to calibrate the power and efficiency of the HHG signals directly output from the CPPLN sample against the mid-IR FW pump light. Remarkably, the overall output power is calculated to be 2.65 mW. When calibrating the insertion loss due to reflection at the liquid nitrogen–air interface, the conversion efficiency of the entire visible band (400–800 nm, covering the 5th–8th HG signals) within the CPPLN sample is about 18.0%, a value much higher than in atomic vapor and plasma. The conversion efficiency of the 4th–8th HG signals is estimated to be 0.7%, 4.5%, 7.2%, 5.1%, and 1.2%, respectively. Another interesting thing is that 6th HG has a much higher efficiency than 4th HG, and even 8th HG is stronger than 4th HG. This clearly confirms the importance of the design and optimization of the QPM bands that have been made in Fig. 2 for enhancing higher order HG.

In summary, we have realized the design and fabrication of a CPPLN nonlinear crystal that offers controllable multiple QPM bands to support 2nd–8th HG simultaneously. Upon illumination of a mid-IR femtosecond pulse laser, we have observed the generation of an ultrabroadband visible white light beam corresponding to 5th–8th HG with a record high conversion efficiency of 18%. The success is attributed to several factors. First, the CPPLN crystal offers a series of broad QPM bands with a considerably large effective nonlinear susceptibility χ_{eff} and freely designated spectral position to support SHG and SFG in the different wavelength bands that are necessary for various-order HHG. Second, these QPM bands cover a broad wavelength band of pump light and thus enable a large fraction of the energy involved in the mid-IR femtosecond pulse laser to participate in the HHG process. Third, all HHG processes are

collinear in this 1D CPPLN sample so that various-order harmonic waves, FW, second harmonic wave, third harmonic wave, etc., are transported along the same direction without a walk-off drawback effect to facilitate a maximum nonlinear optical interaction length and a greatly enhanced efficiency of HHG. Finally, the maximum nonlinear susceptibility component d_{33} is adopted in CPPLN. The CPPLN nonlinear crystal with HHG hints at a very promising means for greatly expanding the power to engineer high-order nonlinear interactions in solid state materials and can find application in supercontinuum generation, ultrafast lasers, frequency combs, large-scale laser displays, and short-wavelength laser sources.

This work is supported by the 973 Program of China, Grants No. 2011CB922002 and No. 2013CB632704, and the National Natural Science Foundation of China, Grant No. 11374357.

*lizy@aphy.iphy.ac.cn

[1] J. A. Armstrong, N. Bloembergen, J. Ducuing, and P. S. Pershan, Interactions between light waves in a nonlinear dielectric, Phys. Rev. **127**, 1918 (1962).
[2] P. A. Franken and J. F. Ward, Optical harmonics and nonlinear phenomena, Rev. Mod. Phys. **35**, 23 (1963).
[3] Y. R. Shen, *The Principles of Nonlinear Optics* (Wiley, New York, 1984).
[4] M. M. Fejer, G. A. Magel, D. H. Jundt, and R. L. Byer, Quasi-phase-matched second harmonic generation: tuning and tolerances, IEEE J. Quantum Electron. **28**, 2631 (1992).
[5] V. Berger, Nonlinear Photonic Crystals, Phys. Rev. Lett. **81**, 4136 (1998).
[6] N. G. R. Broderick, G. W. Ross, H. L. Offerhaus, D. J. Richardson, and D. C. Hanna, Hexagonally Poled lithium Niobate: A Two-Dimensional Nonlinear Photonic Crystal, Phys. Rev. Lett. **84**, 4345 (2000).
[7] A. Arie and N. Voloch, Periodic, quasi-periodic, and random quadratic nonlinear photonic crystals, Laser Photonics Rev. **4**, 355 (2010).
[8] S. N. Zhu, Y.-Y. Zhu, Y.-Q. Qin, H.-F. Wang, C.-Z. Ge, and N.-B. Ming, Experimental Realization of Second Harmonic Generation in a Fibonacci Optical Superlattice of $Litao_3$, Phys. Rev. Lett. **78**, 2752 (1997).
[9] B. Q. Chen, C. Zhang, R. J. Liu, and Z. Y. Li, Multi-direction high-efficiency second harmonic generation in ellipse structure nonlinear photonic crystals, Appl. Phys. Lett. **105**, 151106 (2014).
[10] S. N. Zhu, Y. Y. Zhu, and N. B. Ming, Quasi-phase-matched third-harmonic generation in a quasi-periodic optical superlattice, Science **278**, 843 (1997).
[11] O. Pfister, J. S. Wells, L. Hollberg, L. Zink, D. A. Van Baak, M. D. Levenson, and W. R. Bosenberg, Continuous-wave frequency tripling and quadrupling by simultaneous three-wave mixings in periodically poled crystals: application to a two-step 1.19–10.71-μm frequency bridge, Opt. Lett. **22**, 1211 (1997).
[12] Y. Sheng, D. Ma, M. Ren, B. Chen, V. Roppo, Z. Li, K. Koynov, and W. Krolikowski, Broadband cascading of second-order nonlinearity in randomized nonlinear photonic crystal, J. Phys. D **45**, 365105 (2012).
[13] B. Q. Chen, M.-L. Ren, R.-J. Liu, C. Zhang, Y. Sheng, B.-Q. Ma, and Z.-Y. Li, Simultaneous broadband generation of second and third harmonics from chirped nonlinear photonic crystals, Light Sci. Appl. **3**, e189 (2014).
[14] K. Miyata, V. Petrov, and F. Noack, High-efficiency single-crystal third-harmonic generation in BiB_3O_6, Opt. Lett. **36**, 3627 (2011).
[15] Y. K. Yap, M. Inagaki, S. Nakajima, Y. Mori, and T. Sasaki, High-power fourth- and fifth-harmonic generation of a Nd: YAG laser by means of a $CsLiB_6O_{10}$, Opt. Lett. **21**, 1348 (1996).
[16] X. Zhang, Z. Wang, G. Wang, Y. Zhu, Z. Xu, and C. Chen, Widely tunable and high-average-power fourth-harmonic generation of a Ti:sapphire laser with a $KBe_2BO_3F_2$ prism-coupled device, Opt. Lett. **34**, 1342 (2009).
[17] X. Zhang, L. Wang, X. Wang, G. Wang, Y. Zhu, and C. Chen, High-power sixth-harmonic generation of an Nd: YAG laser with $KBe_2BO_3F_2$ prism-coupled devices, Opt. Commun. **285**, 4519 (2012).
[18] J. F. Ward and G. H. C. New, Optical third harmonic generation in gases by a focused laser beam, Phys. Rev. **185**, 57 (1969).
[19] S. Suntsov, D. Abdollahpour, D. G. Papazoglou, and S. Tzortzakis, Filamentation-induced third-harmonic generation in air via plasma-enhanced third-order susceptibility, Phys. Rev. A **81**, 033817 (2010).
[20] P. St. J. Russell, P. Hölzer, W. Chang, A. Abdolvand, and J. C. Travers, Hollow-core photonic crystal fibres for gas-based nonlinear optics, Nat. Photonics **8**, 278 (2014).
[21] N. Y. Joly, J. Nold, W. Chang, P. Hölzer, A. Nazarkin, G. K. L. Wong, F. Biancalana, and P. St. J. Russell, Bright Spatially Coherent Wavelength-Tunable Deep-UV Laser Source Using an Air-Filled Photonic Crystal Fiber, Phys. Rev. Lett. **106**, 203901 (2011).
[22] A. Paul, R. A. Bartels, R. Tobey, H. Green, S. Weiman, I. P. Christov, M. M. Murnane, H. C. Kapteyn, and S. Backus, Quasi-phase-matched generation of coherent extreme-ultraviolet light, Nature (London) **421**, 51 (2003).
[23] T. Sekikawa, A. Kosuge, T. Kanai, and S. Watanabe, Nonlinear optics in the extreme ultraviolet, Nature (London) **432**, 605 (2004).
[24] S. Hädrich, A. Klenke, J. Rothhardt, M. Krebs, A. Hoffmann, O. Pronin, V. Pervak, J. Limpert, and A. Tünnermann, High photon flux table–top coherent extreme-ultraviolet source, Nat. Photonics **8**, 779 (2014).
[25] A. Ravasio *et al.*, Single-Shot Diffractive Imaging with a Table–Top Femtosecond Soft X-Ray Laser-Harmonics Source, Phys. Rev. Lett. **103**, 028104 (2009).
[26] M. L. Ren, D. L. Ma, and Z. Y. Li, Experimental demonstration of super quasi-phase matching in nonlinear photonic crystal, Opt. Lett. **36**, 3696 (2011).
[27] M. L. Ren and Z. Y. Li, An effective susceptibility model for exact solution of second harmonic generation in general quasi-phase-matched structures, Europhys. Lett. **94**, 44003 (2011).